

Pisces VII/Triangulum III - M33's second dwarf satellite galaxy

Michelle L. M. Collins,¹★ Noushin Karim,¹ David Martinez-Delgado,² Matteo Monelli^{3,4}, Erik J. Tollerud⁵, Giuseppe Donatiello⁶, Mahdiah Navabi¹, Emily Charles¹, Walter Boschin^{3,4,7}

¹*School of Maths and Physics, University of Surrey, Guildford, GU2 7XH, UK*

²*Instituto de Astrofísica de Andalucía, CSIC, Glorieta de la Astronomía, E-18080, Granada, Spain*

³*Instituto de Astrofísica de Canarias (IAC), Calle Vía Láctea s/n, E-38205 La Laguna, Tenerife; Spain*

⁴*Facultad de Física, Universidad de La Laguna, Avda. Astrofísico Fco. Sánchez s/n, 38200 La Laguna, Tenerife, Spain.*

⁵*Space Telescope Science Institute, 3700 San Martin Drive, Baltimore, MD 21218, USA*

⁶*UAI – Unione Astrofili Italiani /P.I. Sezione Nazionale di Ricerca Profondo Cielo, 72024 Oria, Italy*

⁷*Fundación G. Galilei - INAF (Telescopio Nazionale Galileo), Rambla J. A. Fernández Pérez 7, E-38712 Breña Baja (La Palma), Spain*

Accepted XXX. Received YYY; in original form ZZZ

ABSTRACT

Pisces VII/Triangulum III (Pisc VII) was discovered in the DESI Legacy Imaging Survey and was shown to be a Local Group dwarf galaxy with follow-up imaging from the 4-m Telescopio Nazionale Galileo. However, this imaging was unable to reach the horizontal branch of Pisc VII, preventing a precision distance measurement. The distance bound from the red giant branch population placed Pisc VII as either an isolated ultra-faint dwarf galaxy or the second known satellite galaxy of Triangulum (M33). Using deep imaging from Gemini GMOS-N, we have resolved the horizontal branch of Pisc VII, and measure a distance of $D = 916^{+65}_{-53}$ kpc, making Pisc VII a likely satellite of M33. We also remeasure its size and luminosity from this deeper data, finding $r_{\text{half}} = 186^{+58}_{-32}$ pc, $M_V = -6.0 \pm 0.3$ and $L = 2.2^{+0.7}_{-0.5} \times 10^4 L_\odot$. Given its position in the M33 halo, we argue that Pisc VII could support the theory that M33 is on its first infall to the Andromeda system. We also discuss the presence of blue plume and helium burning stars in the colour-magnitude diagram of Pisc VII that are consistent with ages of ~ 1.5 Gyr. If these are truly members of the galaxy, it would transform our understanding of how reionisation affects the faintest galaxies. Future deep imaging and dynamics could allow significant insight into both the stellar populations of Pisc VII and the evolution of M33.

Key words: galaxies: Local Group – galaxies: satellites – galaxies: dwarf-surveys – galaxies: formation

1 INTRODUCTION

With a stellar mass of $3 \times 10^9 M_\odot$ (McConnachie 2012) and a halo mass of $\sim 10^{11} M_\odot$ (Corbelli et al. 2014), the Triangulum galaxy (M33) is the third most massive system in the Local Group. Its recent orbital history is something that has been debated in the literature over the past decade. M33 has long been known to harbour a warped HI gas disk (e.g. Rogstad et al. 1976), and deep imaging from the Pan-Andromeda Archaeological Survey (PAndAS) showed significant warping in its stellar disk and a potential stream between M31 and M33 (McConnachie et al. 2009, 2010). Both features have been attributed to a previous close passage (50–100 kpc) with M31 within the past ~ 3 Gyr (e.g. McConnachie et al. 2009; Putman et al. 2009; Tepper-García et al. 2020). However, other studies using a combination of M33's proper motion and inference from cosmological simulations suggest it is far more likely that M33 is on its first infall to the Andromeda system (e.g. Patel et al. 2017; van der Marel et al. 2019).

These vastly different hypotheses carry significant implications for understanding our nearest neighbour galaxies, for example, their expected satellite systems. Any close passage between M33 and the vastly more massive M31 would have stripped much of M33's dark

and stellar halo, as well as a number of its satellites. This naturally reduces the number of dwarf galaxies we expect to find around M33, which is currently satellite-poor compared to other Local Group spirals. To date, it has only one (mostly) secure satellite candidate – Andromeda (And) XXII (Martin et al. 2009; Chapman et al. 2013) – which has a luminosity of $L = 3.1 \times 10^4 L_\odot$ (Martin et al. 2016; Savino et al. 2022). Yet predictions from cosmological simulations suggest it should harbour $\sim 8 - 10$ dwarf galaxies with $L > 10^4 L_\odot$ (Dooley et al. 2017; Patel et al. 2018a). If M33 did experience a close flyby with M31, this could explain its “missing” satellite issue.

In the first infall scenario, we must instead assume that these satellites exist, but have not been found yet as they lie beneath the detection thresholds of current surveys. This is certainly plausible as the only deep, wide-field survey of M33 is PAndAS (McConnachie et al. 2009, 2018). This survey only probed M33 out to a radius of ~ 50 kpc, which is about a third of its predicted virial radius (e.g. Patel et al. 2018a), and is only sensitive to satellites with $L \gtrsim 2 \times 10^4 L_\odot$ (Doliva-Dolinsky et al. 2022, 2023). Thus, there may be a number of dwarf galaxies waiting to be uncovered both outside and within the PAndAS boundary (Patel et al. 2018a). We cannot know for sure until we have a full, wide and deep survey of the M33 halo.

With this in mind, we have been performing a systematic visual survey of shallow DESI Legacy Imaging Survey (DESI-LIS) data to hunt for faint dwarf galaxies that are too low surface bright-

★ E-mail: m.collins@surrey.ac.uk (MLMC)

ness to be detected with automated routines like match-filter (e.g. Drlica-Wagner et al. 2015; Koposov et al. 2015; Cerny et al. 2021a,b; Doliva-Dolinsky et al. 2022). Our visual inspection survey is complementary to these efforts, as our approach is more sensitive to partially resolved systems which could be missed by the automatic detection algorithms. To date, we have found one M31 dwarf galaxy candidate (Pegasus V, Collins et al. 2022) and one system that is either an isolated Local Group ultra-faint dwarf galaxy (UFD) or the second known satellite of M33 – Pisces VII/Triangulum III (Pisc VII, Martínez-Delgado et al. 2022). Pisc VII was first identified as an over-density of partially resolved sources in DESI-LIS and followed up with the 4-m Telescopio Nazionale Galileo (TNG). Unfortunately, Martínez-Delgado et al. (2022) could not well-constrain its distance.

Our initial imaging also showed that Pisc VII may host stars as young as ~ 1 Gyr based on an over-density of blue stars in its color magnitude diagram. This would be surprising for such a faint ($M_V = -6.1 \pm 0.2$, Martínez-Delgado et al. 2022) dwarf galaxy, as such systems with stellar masses of order $\sim 10^5 M_\odot$ are typically presumed to cease star formation shortly after the epoch of reionisation (e.g. ?????). However, recent observational studies have identified a number of ultra-faint dwarf galaxies with extended star formation. These include the isolated dwarf Pegasus W (McQuinn et al. 2023) and the Andromeda satellite And XIII (?). This may imply our understanding of the impact of reionisation on star formation in low mass galaxies is incomplete, or that these systems have reignited their star formation after reionisation by either retaining or accreting cold gas (e.g. ???).

To determine the distance to Pisc VII and to further shed light on the potential young stellar population in this system, we have acquired deeper Gemini/GMOS-N imaging of Pisc VII that allows us to identify the horizontal branch (HB) of this galaxy. In § 2, we present the details of our imaging before deriving Pisc VII’s structural parameters and distance in § 3. We discuss the implications of our findings in § 4 before concluding in § 5.

2 GEMINI GMOS-N IMAGING

To determine the distance to Pisc VII, we applied for follow-up imaging with the Gemini North GMOS-N instrument (Program ID GN-2022B-Q-132, PI Collins). Pisc VII was observed on 2022-08-08 in the g - and r -band, split into 4×450 s and 4×240 s exposures respectively. The images were reduced using the Gemini DRAGONS package to perform dark, bias and flat fielding, before stacking the resulting images into our final science frames. We next performed photometry using DAOPHOT/ALLFRAME (Stetson 1987, 1994) in largely the same manner as Monelli et al. (2010), Martínez-Delgado et al. (2022) and Collins et al. (2022). We identified stellar sources on each stacked image and performed aperture photometry, PSF derivation and PSF photometry with ALLSTAR. We passed the final list of stars to ALLFRAME to construct catalogues in both g - and r -band before combining the two. Finally, we calibrated our instrumental magnitudes by matching sources to photometry from the Sloan Digital Sky Survey (Abazajian et al. 2009) using linear relation in each band. We then use the data from Schlafly & Finkbeiner (2011) to extinction correct our data in each band, where $A_g = 0.357$ and $A_r = 0.247$.

Star-galaxy separation was performed using the sharpness parameter in each band (requiring $-0.5 < \text{sharp} < +0.5$). In Fig. 1 we present the colour-magnitude diagram (CMD) in the left-hand panel for the central $1.4'$, which corresponds to two times the half-light radius (see § 3.1). The right-hand panel shows an equal area annulus

located beyond three half-light radii for the candidate. A sparse red giant branch (RGB) is seen in CMD for the source, as well as a horizontal branch (HB) feature at $g \sim 25.5$. Corresponding features are not seen in the field CMD.

3 RESULTS

In this section, we present the structural parameters, distance and luminosity for Pisc VII. We summarise these findings in Table 1. Our data analysis was conducted using Python, and relies heavily on packages including ASTROPY (Astropy Collaboration et al. 2013, 2018, 2022); EMCEE (Foreman-Mackey et al. 2013), CORNER (Foreman-Mackey 2016), NUMPY (Harris et al. 2020), SCIPY (Virtanen et al. 2020) and MATPLOTLIB (Hunter 2007).

3.1 Re-measuring the structural properties of Pisc VII

We measured structural properties and luminosities for Pisc VII from our shallower TNG data. However, our deeper Gemini data allow us to update and refine these values. We follow the same method as presented in Martínez-Delgado et al. (2022) and Collins et al. (2022). This method is based on the approach of Martin et al. (2016), where we assume that our Gemini observations contain a dwarf galaxy candidate with N_* observed members whose surface brightness profile can be modelled as an exponentially declining function with half-light radius r_{half} and an ellipticity ϵ :

$$\rho_{\text{dwarf}}(r) = \frac{1.68^2}{2\pi r_{\text{half}}^2 (1 - \epsilon)} N_* \exp\left(\frac{-1.68r}{r_{\text{half}}}\right) \quad (1)$$

where r is the elliptical radius such that:

$$r = \left(\left(\frac{1}{1 - \epsilon} ((x - x_0) \cos \theta - (y - y_0) \sin \theta) \right)^2 + \left((x - x_0) \sin \theta - (y - y_0) \cos \theta \right)^2 \right)^{\frac{1}{2}}. \quad (2)$$

Here, θ is the position angle of the major axis, x_0 and y_0 are the central co-ordinates of the dwarf galaxy and x and y are the coordinates on the tangent plane to the sky at the center of the Gemini GMOS-N field. We then assume that it is located in a field with a contaminant population that is uniform in density, described by Σ_b . We can determine Σ_b by subtracting the total number of dwarf galaxy stars (determined from the integral of the surface density profile in Eq. 1) from the total number of potential member stars within the field. We combine these assumptions into a likelihood function:

$$\rho_{\text{model}}(r) = \rho_{\text{dwarf}}(r) + \Sigma_b. \quad (3)$$

which we can sample using a Markov Chain Monte Carlo (MCMC) approach. As in prior work, we use the EMCEE sampler (Foreman-Mackey et al. 2013) to sample the posterior. We use limited uniform priors, requiring only that the number of stars within the dwarf galaxy $N_* \geq 0$, the position angle falls in the range $0 < \theta < \pi$ and the ellipticity lies between $0 < \epsilon < 1$.

Before running EMCEE, we apply cuts to our data to ensure we only include sources down to our approximate completeness limit and to well-sample the contaminating population. We set a wide colour cut of $-0.2 < g - r < 2$, and only include sources with $r < 26$ -mag.

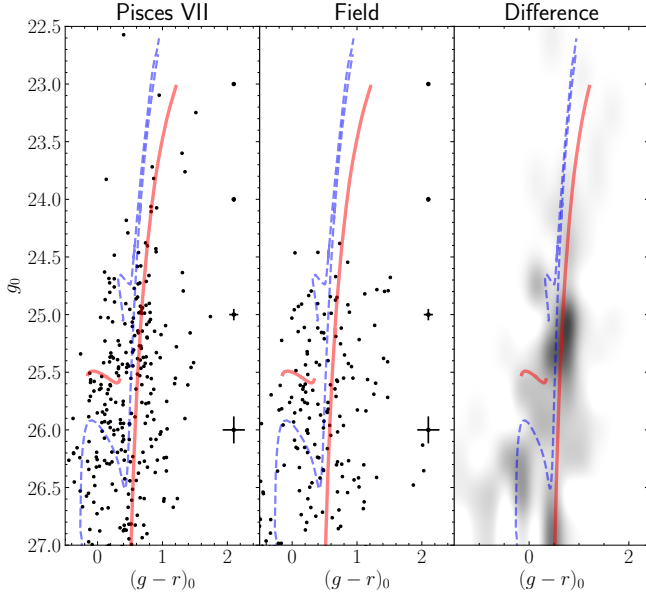


Figure 1. Here we present the deep Gemini-GMOS-N color magnitude diagram for Pisc VII. On the left, we show all stellar sources within $2 \times r_{\text{half}}$, and in the centre we show an equal area annulus beyond $3 \times r_{\text{half}}$. Finally, the right panel shows a Hess diagram where we have subtracted the field CMD from the source CMD. The RGB of Pisc VII can be identified, as well as a horizontal branch feature at $g \sim 25.5$ mag. We overlay two isochrones from the BaSTI library (Hidalgo et al. 2018) with a metallicity of $[\text{Fe}/\text{H}] = -1.9$ dex, an alpha abundance of $[\alpha/\text{Fe}] = +0.4$ and ages of 12.5 Gyr (red solid line) and 1.5 Gyr (blue dashed line). Both isochrones have been shifted to match the CMD by assuming a distance of 952 kpc. Intriguingly, the CMD shows an abundance of blue stars that are well traced by the younger isochrone in Pisc VII which are not seen in the field comparison, as well as potential helium-burning stars above the HB of Pisc VII. Such young stars in an ultra-faint dwarf are completely unexpected, and if validated would have implications for our understanding of reionisation.

We have modified both these cuts and find that our solutions are stable to shallower and narrower cuts. We include all sources within $2.5'$ of the centre. We initialise EMCEE with 100 walkers, and run for 10,000 iterations with a burn in of 3,250. These numbers were determined based on a visual inspection of the traces. We show the results in Fig. 2 and summarise them in Table 1. The solution is well-constrained, localising an over-density at $\text{RA} = 01:21:40.6$, $\text{Dec} = 26:23:28$, with $r_{\text{half}} = 0.67^{+0.2}_{-0.1}$. There are not enough sources to reliably constrain the ellipticity, so we can only place a limit based on the 84% confidence interval, giving $\epsilon < 0.1$. Our results are entirely consistent with – but more precise than – the results of Martínez-Delgado et al. (2022).

3.2 The distance to Pisc VII

In our prior work, we tried to constrain the distance to Pisc VII using its RGB stars. Given the paucity of bright stars in this galaxy, we were not able to make a precise measurement, finding that Pisc VII was located at a distance of $\sim 0.8 - 1$ Mpc. However, our deeper data resolves a HB feature for Pisc VII at $g \sim 25.5$ -mag (see Fig. 1) which we can use as a distance indicator. First, we convert our SDSS photometry into the Johnson BVR magnitude system using the colour transformations of Jordi et al. (2006), as the HB in the V -band has a

Table 1. The final structural and photometric properties for Pisc VII.

Property	Value
RA ($^{\circ}$)	20.419 ± 0.000
dec ($^{\circ}$)	26.391 ± 0.001
r_{half} ($'$)	$0.67^{+0.2}_{-0.1}$
r_{half} (pc)	186^{+58}_{-32}
ϵ	< 0.1
PA ($^{\circ}$)	96^{+32}_{-36}
N_*	69^{+20}_{-18}
$(m-M)_0$	24.8 ± 0.2
D (kpc)	916^{+65}_{-53}
D_{M33} (kpc)	97 ± 6
M_g	-5.7 ± 0.3
M_r	-6.2 ± 0.3
M_V	-6.0 ± 0.3
$L(L_{\odot})$	$2.2^{+0.7}_{-0.5} \times 10^4$

near constant luminosity. Thus, by measuring the HB magnitude in the V -band, we can constrain the distance to Pisc VII.

We employ an MCMC approach to isolate the apparent magnitude of the HB in the V -band by fitting its luminosity function. Similar to the procedure of Weisz et al. (2019); Collins et al. (2022) and McQuinn et al. (2023), we construct a likelihood function to capture the shape of the luminosity function such that:

$$\mathcal{L} = e^{A(V_i - V_{\text{HB}})} + e^{-0.5[(V_i - V_{\text{HB}})/C]^2} \quad (4)$$

where V_i is the V -band magnitude of the i -th star and V_{HB} is the best fitting magnitude for the HB. A , B and C are free parameters. We use flat priors for all three, requiring $0 < A, B, C < 2$. We initialise EMCEE with 100 walkers, and run for 6,000 iterations with a burn in of 3,000. When marginalising over our free parameters, we measure $V_{\text{HB}} = 25.3 \pm 0.1$.

To convert this into a distance measure, we calculate the expected absolute magnitude of the HB using the metallicity dependent calibration of ?, where

$$M_{V,\text{HB}} = (0.13 \pm 0.09) * ([\text{Fe}/\text{H}] + 1.5) + (0.54 \pm 0.07). \quad (5)$$

We use a value of $[\text{Fe}/\text{H}] = -1.9 \pm 0.2$ dex based on our best fit isochrone to the Pisc VII CMD, where the uncertainty is based on inspecting isochrones of higher and lower metallicity against the data. These values give $M_{V,\text{HB}} = 0.49^{+0.08}_{-0.04}$. Combining this with our measured apparent magnitude of $V_{\text{HB}} = 25.3 \pm 0.1$ we calculate a heliocentric distance for Pisc VII of $D = 916^{+65}_{-53}$ kpc.

Now that we have 3D coordinates for Pisc VII, we can also place it in the wider context of the Andromeda-Triangulum group. Using the coordinates and distance for M31 and M33 from Savino et al. (2022) ($D = 859^{+24}_{-23}$ kpc and 859^{+24}_{-23} kpc respectively) we measure these as $D_{\text{M31}} = 285^{+21}_{-18}$ kpc and $D_{\text{M33}} = 97 \pm 6$ kpc for M31 and M33. If we assume the virial radius of M31 is $\sim 250 - 300$ kpc, (e.g. Patel et al. 2018b; Kafle et al. 2018; Blańa Díaz et al. 2018) and M33 is $r_{200} \sim 160$ kpc (Patel et al. 2018a), we see that Pisc VII lies comfortably within the halo of M33, and in the outskirts of Andromeda's. It is thus a likely satellite of M33. We discuss this further in § 4.

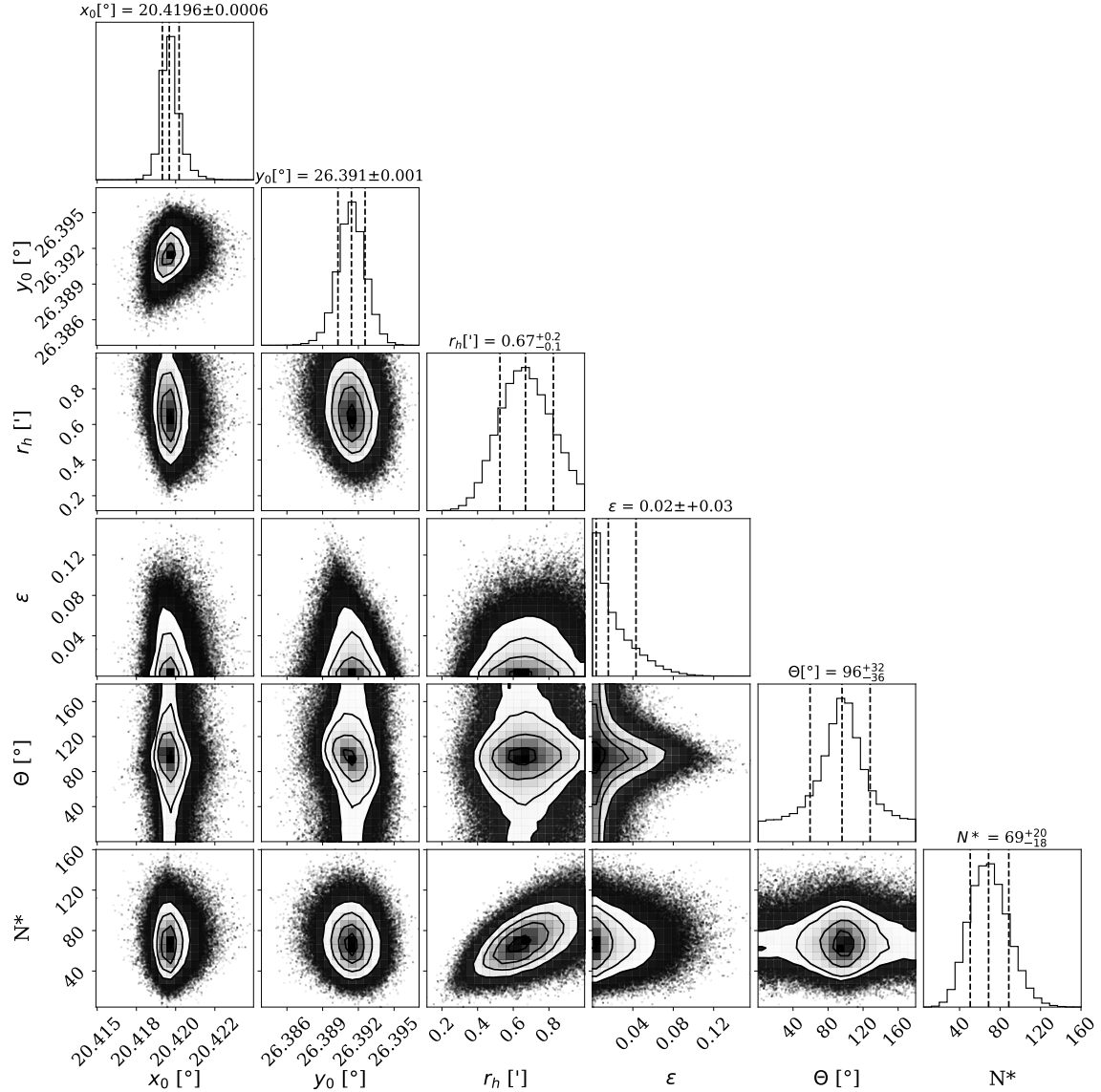


Figure 2. Here we show the posteriors for the structural properties of Pisc VII, derived using EMCEE (Foreman-Mackey et al. 2013). All properties other than the ellipticity (ϵ) are well-constrained. These values are all consistent with our previous results presented in Martínez-Delgado et al. (2022) within 1σ . The precision has improved.

3.3 The luminosity of Pisc VII

Armed with a distance, we can now place a tighter constraint on the total luminosity of Pisc VII. In Martínez-Delgado et al. (2022) we measured this to range from $-6.1 < M_V < -7.0$, depending on its distance. With the improved precision on our distance, we can reevaluate this with our deeper data. We follow the same method as Martínez-Delgado et al. (2022) and Collins et al. (2022), which is again based on the procedure outlined in Martin et al. (2016). We begin by downloading the luminosity function and corresponding isochrone for an old (age of 12.5 Gyr), metal-poor ($[\text{Fe}/\text{H}] = -1.9$) stellar population from the PARSEC database. We use the luminosity function as a probability distribution function (PDF) for the stellar population of Pisc VII. We shift the isochrone to the presumed distance of Pisc VII and use the PDF to perform a probability-weighted random selection of a magnitude in the g -band, and its corresponding r -band magnitude. We continue to select magnitudes until we

have collected N_* values that fall within the colour cuts we used to measure the structural properties of Pisc VII (see § 3.1 for details). Once we have recorded N_* values in this region, we then sum the magnitudes for all stars selected both within and outside of this cut to obtain final magnitudes in the g and r -band. To account for shot noise and uncertainties in N_* and distance, we repeat this procedure 1000 times, selecting a different value for distance and N_* each time by randomly drawing from a Gaussian centered on our best fit values, with a width equal to their uncertainties.

The results from this procedure are $M_g = -5.7 \pm 0.3$ and $M_r = -6.2 \pm 0.3$. We can then translate these to an absolute magnitude in the V -band of $M_V = -6.0 \pm 0.3$ using the colour transforms of Jordi et al. (2006). As Pisc VII is so faint and low density, its stellar populations are uncrowded down to below the HB, so we apply no completeness corrections to these measured values. Our new luminosity is fully consistent with the value we reported in Martínez-Delgado et al. (2022). Translating this into a luminosity,

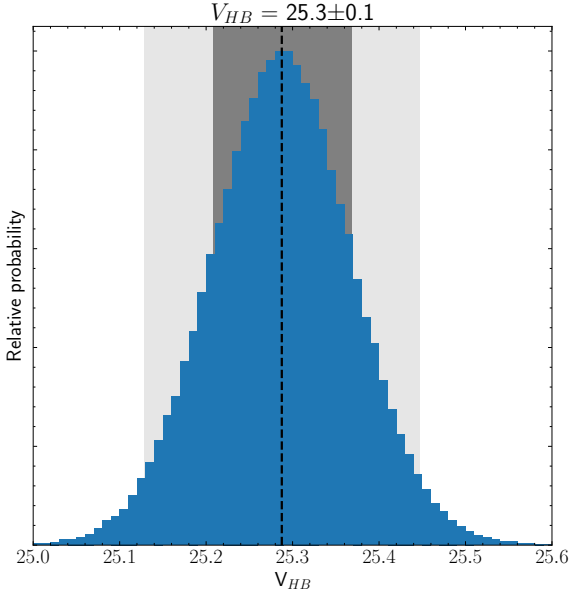


Figure 3. This figure shows the marginalised probability distribution for the apparent magnitude of the horizontal branch of Pisc VII, g_{HB} . The dashed line shows the median value, while the shaded gray regions show the 1 and 2σ uncertainties.

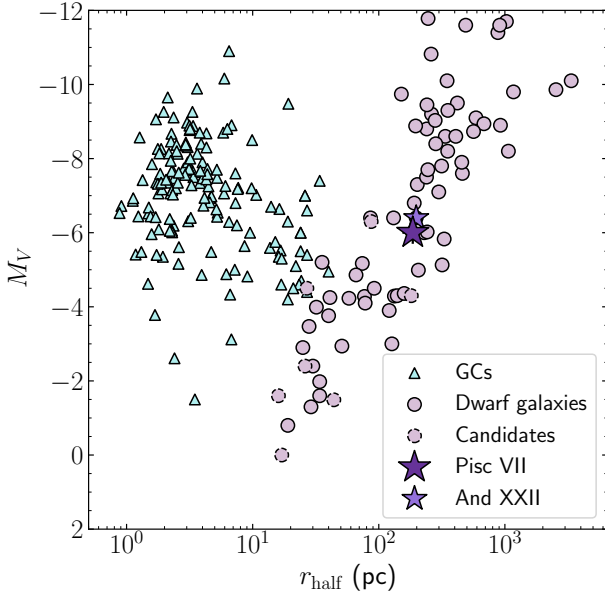


Figure 4. Above we show the size-luminosity parameter space for dwarf galaxies (light pink circles), dwarf candidates (pink circles with dashed borders) and globular clusters (turquoise triangles). Pisc VII is highlighted as the dark purple star, and M33's other potential satellite – And XXII – is shown as a smaller, light purple star.

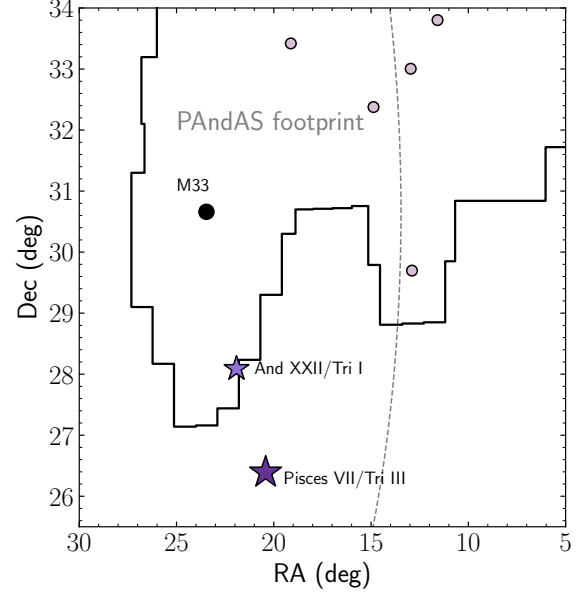


Figure 5. Here we show the location of Pisc VII (dark purple star) in the Triangulum system. Located outside the PAndAS footprint (shown as the black outline), it is closer in projection and 3D distance to M33 (labelled) than M31. The approximate virial radius of M33 is shown as a dashed gray line. We also show M33's other possible satellite, And XXII, as a light purple star. Interestingly, the two dwarf galaxies appear to be in a direct line from M33. Other M31 dwarf galaxies in this region are shown as light pink circles.

we measure $L = 2.2^{+0.7}_{-0.5} \times 10^4 L_{\odot}$. Given the size and luminosity we measure for Pisc VII, it is a highly probable ultra faint dwarf galaxy rather than a stellar cluster. In Fig. 4, we show the half-light radii for dwarf galaxies (pink circles), candidate dwarf galaxies (pink circles with dashed border) and globular clusters (turquoise triangles) vs. their absolute magnitude (with data taken from Harris 1996; Mackey et al. 2013; Koposov et al. 2015; Martin et al. 2016; Martínez-Vázquez et al. 2019; Simon et al. 2020; Cerny et al. 2021a,b, 2022, 2023; Savino et al. 2022). Pisc VII (dark purple star) is clearly found in the dwarf galaxy regime, and significantly offset from globular clusters of comparable luminosity. To definitively test this, we would require spectroscopy to measure any dark matter contribution and/or a spread in metallicity characteristic of a dwarf galaxy.

4 DISCUSSION

4.1 Pisc VII – a satellite of M31 or M33?

With our revised distance of $D = 916^{+65}_{-53}$ kpc, we have shown that Pisc VII is unlikely to be an isolated ultra-faint at the present day. At a distance of $D_{M33} = 97 \pm 6$ kpc from Triangulum, it is comfortably within its predicted dark matter halo (Patel et al. 2018a) and therefore a likely M33 satellite. However, with a distance from the centre of M31 of $D_{M31} = 285^{+21}_{-18}$ kpc, it could be a far-flung Andromeda satellite. A bulk radial velocity for Pisc VII would likely resolve this ambiguity and be able to determine for sure which of M33 and M31. We visualise the projected location of Pisc VII from both galaxies in Fig. 5.

The proximity of Pisc VII to M33 is interesting, as to-date, M33 has only one known satellite – And XXII – which is close to M33 in

projection (~ 43 kpc). Recent work from [Savino et al. \(2022\)](#) find it has a 3D separation from M33 of 113^{+31}_{-30} kpc and a separation from M31 of 215 ± 9 kpc, making its membership more ambiguous than Pisc VII. However, based on its radial velocity, [Chapman et al. \(2013\)](#) argued it is energetically more likely to be a satellite of M33. M33 is predicted to have 8 satellites with a luminosity equivalent to $10^4 L_{\odot}$ or greater ([Dooley et al. 2017](#); [Patel et al. 2018a](#)) within its virial radius. While Pisc VII adds a valuable second data point to M33's satellite system, it retains a missing satellite problem. However, there is cause for optimism. Given that this satellite falls outside the deep PAndAS survey region (which covers only half the virial radius of M33), its existence implies that there may be a wealth of faint dwarf galaxies in the ultra-faint regime awaiting our discovery.

4.2 Constraining the orbital history of M33

If we assume Pisc VII (and And XXII) are bound to M33, we can further address the issue of M33's recent orbital history. Given its warped HI (e.g. [Rogstad et al. 1976](#)) and stellar disks (e.g. [McConnachie et al. 2009](#)) it has been proposed that M33 has experienced a prior close passage (< 100 kpc) with M31 a few Gyr ago ([McConnachie et al. 2009](#); [Putman et al. 2009](#); [Tepper-García et al. 2020](#)). However this is in tension with the proper motion informed orbital history of M33 which suggests it is on first infall and that a close passage with M31 in the past 3 Gyr is rare (less than 1% chance, [Patel et al. 2017](#); [van der Marel et al. 2019](#)). In this case, the warps must be caused via some other method such as repeated close passages of satellites with M33 ([Starkenburg et al. 2016](#)), asymmetric gas accretion, or long range tidal forces from M31. The first of these suggestions requires M33 to have a significant population of satellites, something which is not yet observed.

If there truly was a close passage between M31 and M33 a few Gyr ago, much of its halo (and thus satellites) would have been stripped by M31. Any remaining satellites would likely be found close to M33. Given both Pisc VII and And XXII are found at a large distance from M33 (> 100 kpc), this would seem to support the model of a first infall rather than a close encounter. In this context, dynamics and proper motions for Pisc VII are very desirable so we could both confirm it is bound to M33, and ascertain whether Pisc VII could have induced warps in M33's disks. Based on our CMD (Fig. 1) there are a handful of stars in Pisc VII that would be bright enough to obtain spectra for with e.g. the 10 m Keck telescopes. Proper motions can only be acquired with multi-epoch observations from space-based telescopes such as Hubble or JWST. Hopefully, such future observations will allow us to solve these multiple mysteries of M33's evolution.

4.3 Blue stars in the CMD of Pisc VII – recent star formation?

Finally, we briefly discuss the presence of blue stars in the CMD just faint-ward of the HB of Pisc VII, as well as the potential helium-burning stars just above the HB. The latter indicate a stellar population within the galaxy with an age of ~ 1 Gyr. Both populations are far more numerous in the dwarf galaxy than in the comparison field (Fig. 1). They are reminiscent of a similar population seen in shallow HST imaging for the newly discovered isolated UFD, Pegasus W ([McQuinn et al. 2023](#)), which are consistent with a young ($\sim 0.5 - 1$ Gyr) population. We overlay a younger isochrone in Fig. 1 and find that these stars are consistent with an age of 1.5 Gyr. They could also be blue stragglers, which are main-sequence stars that have undergone a binary merger or mass transfer event which has

changed their intrinsic colours, shifting them off the main sequence. However, if they truly are younger stars with ages $\sim 1-2$ Gyr, Pisc VII would be the faintest dwarf galaxy to have star formation that has occurred significantly beyond reionisation and would transform our understanding of how UFDs are quenched during this epoch.

5 CONCLUSIONS

In this work, we have reassessed the properties of Pisc VII/Tri III using deep Gemini GMOS-N imaging. We find its structural properties are in good agreement with our previous study from shallower data ([Martínez-Delgado et al. 2022](#)). Specifically, we measure its positions as RA = 01:21:40.6, Dec = 26:23:28, and a half-light radius of $r_{\text{half}} = 186^{+58}_{-32}$ pc. We measure a slightly lower luminosity of $L = 2.2^{+0.7}_{-0.5} \times 10^4 L_{\odot}$ ($M_V = -6.0 \pm 0.3$) which is consistent with previous work within 2σ . Based on its size and luminosity, we conclude Pisc VII is a highly probable dwarf galaxy. Our deep data also allows us to determine the distance to Pisc VII from its horizontal branch of $D = 916^{+65}_{-53}$ kpc. This locates it at a 3D distance of $D_{\text{M33}} = 97 \pm 6$ kpc within the halo of M33 making Pisc VII a highly probable satellite of this system.

Pisc VII is only the second known satellite of M33 and its location at a large distance from M33 may favour a first infall scenario for the orbital history of M33. Proper motions and dynamics would help to determine whether Pisc VII is definitively bound to M33, and thus whether it truly supports the first infall scenario over a prior close encounter with Andromeda. They would also allow us to trace its orbital history to determine whether its past orbit could have induced warps in either its gas or stellar disk.

The detection of a second far-flung satellite of M33 also supports the existence of a wider satellite system for this galaxy. Beyond the PAndAS footprint, shallow survey data make detections of ultra-faints like Pisc VII extremely challenging. A deep, wide-field survey with an instrument like Hyper-Suprime Cam on the 8-m Subaru telescope that covers the extent of its halo would likely uncover a wealth of substructure in this system, and would definitively assess whether or not M33 has a missing satellite problem.

Finally, we comment on blue stars in the CMD that are consistent with a younger age population (1-2 Gyr). This evidence of recent star formation in such a faint galaxy would be an extremely important finding if verified. Future deep imaging would allow us to study this intriguing population in more detail.

ACKNOWLEDGEMENTS

We thank the anonymous referee for their helpful and constructive comments, which improved the quality of this work. DMD acknowledges financial support from the Talentia Senior Program (through the incentive ASE-136) from Secretaría General de Universidades, Investigación y Tecnología, de la Junta de Andalucía. DMD acknowledges funding from the State Agency for Research of the Spanish MCIU through the "Center of Excellence Severo Ochoa" award to the Instituto de Astrofísica de Andalucía (SEV-2017-0709) and project (PDI2020-114581GB-C21/AEI/10.13039/501100011033).

M.M. acknowledges support from the Agencia Estatal de Investigación del Ministerio de Ciencia e Innovación (MCIN/AEI) under the grant "RR Lyrae stars, a lighthouse to distant galaxies and early galaxy evolution" and the European Regional Development Fund (ERDF) with reference PID2021-127042OB-I00.

Based on observations obtained at the international Gemini Observatory, a program of NSF's NOIRLab, which is managed by the Association of Universities for Research in Astronomy (AURA) under a cooperative agreement with the National Science Foundation on behalf of the Gemini Observatory partnership: the National Science Foundation (United States), National Research Council (Canada), Agencia Nacional de Investigación y Desarrollo (Chile), Ministerio de Ciencia, Tecnología e Innovación (Argentina), Ministério da Ciência, Tecnologia, Inovações e Comunicações (Brazil), and Korea Astronomy and Space Science Institute (Republic of Korea). Processed using the Gemini DRAGONS (Data Reduction for Astronomy from Gemini Observatory North and South) package.

This work was enabled by observations made from the Gemini North telescope, located within the Maunakea Science Reserve and adjacent to the summit of Maunakea. We are grateful for the privilege of observing the Universe from a place that is unique in both its astronomical quality and its cultural significance.

DATA AVAILABILITY

Raw images and their associated calibrations are stored on the Gemini archive and are publicly available. Our fully reduced photometric catalogue is available upon reasonable request to the lead author.

REFERENCES

- Abazajian K. N., et al., 2009, *ApJS*, **182**, 543
- Astropy Collaboration et al., 2013, *A&A*, **558**, A33
- Astropy Collaboration et al., 2018, *AJ*, **156**, 123
- Astropy Collaboration et al., 2022, *apj*, **935**, 167
- Besla G., Kallivayalil N., Hernquist L., Robertson B., Cox T. J., van der Marel R. P., Alcock C., 2007, *ApJ*, **668**, 949
- Blaña Díaz M., et al., 2018, *MNRAS*, **481**, 3210
- Cerny W., et al., 2021a, *ApJ*, **910**, 18
- Cerny W., et al., 2021b, *ApJ*, **920**, L44
- Cerny W., et al., 2022, *arXiv e-prints*, p. arXiv:2209.12422
- Cerny W., et al., 2023, *ApJ*, **942**, 111
- Chapman S. C., et al., 2013, *MNRAS*, **430**, 37
- Collins M. L. M., Charles E. J. E., Martínez-Delgado D., Monelli M., Karim N., Donatiello G., Tollerud E. J., Boschín W., 2022, *MNRAS*, **515**, L72
- Corbelli E., Thilker D., Zibetti S., Giovanardi C., Salucci P., 2014, *A&A*, **572**, A23
- Deason A. J., et al., 2021, *MNRAS*, **501**, 5964
- Doliva-Dolinsky A., et al., 2022, *ApJ*, **933**, 135
- Doliva-Dolinsky A., et al., 2023, *arXiv e-prints*, p. arXiv:2303.01528
- Dooley G. A., Peter A. H. G., Yang T., Willman B., Griffen B. F., Frebel A., 2017, *MNRAS*, **471**, 4894
- Drlica-Wagner A., et al., 2015, *ApJ*, **813**, 109
- Erkal D., et al., 2019, *MNRAS*, **487**, 2685
- Erkal D., Belokurov V. A., Parkin D. L., 2020, *MNRAS*, **498**, 5574
- Erkal D., et al., 2021, *MNRAS*, **506**, 2677
- Foreman-Mackey D., 2016, *The Journal of Open Source Software*, **1**, 24
- Foreman-Mackey D., Hogg D. W., Lang D., Goodman J., 2013, *PASP*, **125**, 306
- Garavito-Camargo N., Besla G., Laporte C. F. P., Johnston K. V., Gómez F. A., Watkins L. L., 2019, *ApJ*, **884**, 51
- Garavito-Camargo N., Besla G., Laporte C. F. P., Price-Whelan A. M., Cunningham E. C., Johnston K. V., Weinberg M., Gómez F. A., 2021, *ApJ*, **919**, 109
- Gómez F. A., Besla G., Carpinero D. D., Villalobos Á., O'Shea B. W., Bell E. F., 2015, *ApJ*, **802**, 128
- Harris W. E., 1996, *AJ*, **112**, 1487
- Harris C. R., et al., 2020, *Nature*, **585**, 357
- Hidalgo S. L., et al., 2018, *ApJ*, **856**, 125
- Hunter J. D., 2007, *Computing in Science & Engineering*, **9**, 90
- Irwin M. J., et al., 2007, *ApJ*, **656**, L13
- Jordi K., Grebel E. K., Ammon K., 2006, *A&A*, **460**, 339
- Kafle P. R., Sharma S., Lewis G. F., Robotham A. S. G., Driver S. P., 2018, *MNRAS*, **475**, 4043
- Koposov S. E., Belokurov V., Torrealba G., Evans N. W., 2015, *ApJ*, **805**, 130
- Lilleengen S., et al., 2023, *MNRAS*, **518**, 774
- Mackey A. D., et al., 2013, *ApJ*, **770**, L17
- Makarov D., Khoperskov S., Makarov D., Makarova L., Libeskind N., Salomon J.-B., 2023, *MNRAS*, **521**, 3540
- Martin N. F., et al., 2009, *ApJ*, **705**, 758
- Martin N. F., et al., 2016, *ApJ*, **833**, 167
- Martínez-Delgado D., Karim N., Charles E. J. E., Boschín W., Monelli M., Collins M. L. M., Donatiello G., Alfaro E. J., 2022, *MNRAS*, **509**, 16
- Martínez-Vázquez C. E., et al., 2019, *MNRAS*, **490**, 2183
- McConnachie A. W., 2012, *AJ*, **144**, 4
- McConnachie A. W., et al., 2009, *Nature*, **461**, 66
- McConnachie A. W., Ferguson A. M. N., Irwin M. J., Dubinski J., Widrow L. M., Dotter A., Ibata R., Lewis G. F., 2010, *ApJ*, **723**, 1038
- McConnachie A. W., et al., 2018, *ApJ*, **868**, 55
- McQuinn K. B. W., Mao Y.-Y., Buckley M. R., Shih D., Cohen R. E., Dolphin A. E., 2023, *ApJ*, **944**, 14
- Monelli M., et al., 2010, *ApJ*, **720**, 1225
- Patel E., Besla G., Sohn S. T., 2017, *MNRAS*, **464**, 3825
- Patel E., Carlin J. L., Tollerud E. J., Collins M. L. M., Dooley G. A., 2018a, *MNRAS*, **480**, 1883
- Patel E., Besla G., Mandel K., Sohn S. T., 2018b, *ApJ*, **857**, 78
- Petersen M. S., Peñarrubia J., 2020, *MNRAS*, **494**, L11
- Putman M. E., et al., 2009, *ApJ*, **703**, 1486
- Rogstad D. H., Wright M. C. H., Lockhart I. A., 1976, *ApJ*, **204**, 703
- Savino A., et al., 2022, *ApJ*, **938**, 101
- Schlafly E. F., Finkbeiner D. P., 2011, *ApJ*, **737**, 103
- Simon J. D., et al., 2020, *ApJ*, **892**, 137
- Starkenbourg T. K., Helmi A., Sales L. V., 2016, *A&A*, **595**, A56
- Stetson P. B., 1987, *PASP*, **99**, 191
- Stetson P. B., 1994, *PASP*, **106**, 250
- Tepper-García T., Bland-Hawthorn J., Li D., 2020, *MNRAS*, **493**, 5636
- Vasiliev E., Belokurov V., Erkal D., 2021, *MNRAS*, **501**, 2279
- Vera-Ciro C., Helmi A., 2013, *ApJ*, **773**, L4
- Virtanen P., et al., 2020, *Nature Methods*, **17**, 261
- Weisz D. R., et al., 2019, *MNRAS*, **489**, 763
- van der Marel R. P., Fardal M. A., Sohn S. T., Patel E., Besla G., del Pino A., Sahlmann J., Watkins L. L., 2019, *ApJ*, **872**, 24

This paper has been typeset from a \LaTeX file prepared by the author.